Journal of Geotechnical and Geoenvironmental Engineering, Vol. 136, No. 5, pp. 728-740, 2010

Prediction of permanent deformations in pavements using a high-cycle accumulation model

T. Wichtmann[i)] H. A. Rondón[ii)] A. Niemunis[iii)] Th. Triantafyllidis[iv)] A. Lizcano[v)]

Abstract: The present paper discusses the application of a high-cycle accumulation (HCA) model originally developed for sand for the prediction of permanent deformations in unbound granular material (UGM) used for base and subbase layers in pavements. Cyclic triaxial tests on pre-compacted samples of an UGM have been performed in order to validate and calibrate the model. The stress amplitude, the initial density and the average stress were varied. The test results are compared to those of air-pluviated samples of sand (subgrade material). Some significant differences in the behavior of both materials under cyclic loading are outlined. It is demonstrated that the functions describing the intensity of accumulation can be maintained for UGM with different material constants, but that the flow rule must be generalized in order to describe anisotropy. Recalculations of the laboratory tests show a good prediction of the modified HCA model.

CE Database subject headings: Pavements; Unbound granular material (UGM); Permanent deformations; High-cycle accumulation model; Cyclic triaxial tests

1 Introduction

Traffic loading leads to permanent deformations in the base and subbase layers and in the subgrade of pavements. Even small rates of deformation accumulation may lead to significant settlements after several years of operation.

In order to predict the permanent deformations in pavements empirical equations have been developed. The formulas usually give the vertical strain ε_1 or the settlement s as a function of the number of cycles N. More recent equations (e.g. Huurman [10], Werkmeister et al. [32], Gidel et al. [7], Uzan [30], see also the review by Rondón & Reyes [22]) consider the influence of the stress path during the cycles. However, most of the equations are applicable to very simple cases only, that means to soil layers under level ground subjected to one-dimensional cycles where the minimum deviatoric stress during the cycles is zero. Except the formulas based on large-scale tests (e.g. using a so-called High Vehicle Simulator), the multi-dimensionality of the stress or strain path in the soil is not considered.

The common empirical formulas may suffice for the simple one-dimensional case. However, for more complicated boundary value problems (e.g. the transition zone of a pavement and a bridge abutment) these equations are too simple and more general prediction tools are necessary. The high-cycle accumulation (HCA) model proposed by Niemunis et al. [20] (Section 3) along with the finite element method (FEM) and an "explicit" or "N-type" calculation strategy (Section 2) may serve as such a tool.

The HCA model was originally developed for sand. It predicts the permanent deformations due to a high-cyclic loading, that means a loading with a large number of cycles $N > 10^3$ and with small strain amplitudes $\varepsilon^{\text{ampl}} < 10^{-3}$. It has been validated and calibrated for various sands with different grain size distribution curves (Wichtmann et al. [37]).

The present paper discusses an application of the HCA model to an unbound granular material (UGM) used for base and subbase layers in pavements. For that purpose cyclic triaxial tests have been performed on a typical UGM (Section 4). The amplitude, the initial density and the average stress have been varied. The experimental results are compared to those for a medium-coarse to coarse sand (Section 5). Necessary modifications of the HCA model for an application to the UGM are discussed. A good prediction of the experimental data by the modified HCA model is demonstrated by means of recalculations of the laboratory tests (Section 6).

Readers familiar with the explicit calculation strategy and with the HCA model may skip the next two sections containing a review and may continue with Section 4.

2 Explicit calculation strategy

Two different calculation strategies can be used for finite element (FE) calculations of boundary value problems with cyclic loading. The first one is called "pure implicit". It is illustrated for a shallow foundation in Fig. 1a. Each cycle is calculated with many increments using a conventional constitutive model formulated in terms of the rates of stress ($\dot{\boldsymbol{\sigma}}$) and strain ($\dot{\boldsymbol{\varepsilon}}$). Elastoplastic multi-surface models [3, 18] or the hypoplastic model with intergranular strain [19, 31] may be used for that purpose. The accumulation of permanent deformations results from the fact that the stress-strain-loops are not perfectly closed. The pure implicit strategy is suitable only for small numbers of cycles ($N < 50$). For larger numbers of cycles the numerical error becomes excessive (Niemunis et al. [20]), let alone the large calculation effort.

For large numbers of cycles another calculation strategy is necessary. It is shown in Fig. 1b. Only a few cycles are

[i)] Research Assistant, Institute of Soil Mechanics and Rock Mechanics, University of Karlsruhe, Germany (corresponding author). Email: torsten.wichtmann@ibf.uka.de

[ii)] Research Assistant, Department of Civil and Environmental Engineering. Los Andes University, Bogotá D. C. (Colombia)

[iii)] Research Assistant, Institute of Soil Mechanics and Rock Mechanics, University of Karlsruhe, Germany

[iv)] Professor and Director of the Institute of Soil Mechanics and Rock Mechanics, University of Karlsruhe, Germany

[v)] Professor, Department of Civil and Environmental Engineering. Los Andes University, Bogotá D. C. (Colombia)

calculated implicitly with many strain increments. Larger packages of cycles between are calculated "explicitly". The explicit parts of the calculation require a constitutive formulation which takes packages of cycles ΔN as input and which predicts the permanent strain due to these packages directly, without tracing the oscillating strain path during the individual cycles. Such a constitutive formulation is called "high-cycle accumulation (HCA) model". The external load is kept constant during the explicit parts of the calculation. Therefore, the accumulation of permanent strain due to cyclic loading is treated similarly as a creep deformation in viscoplastic models.

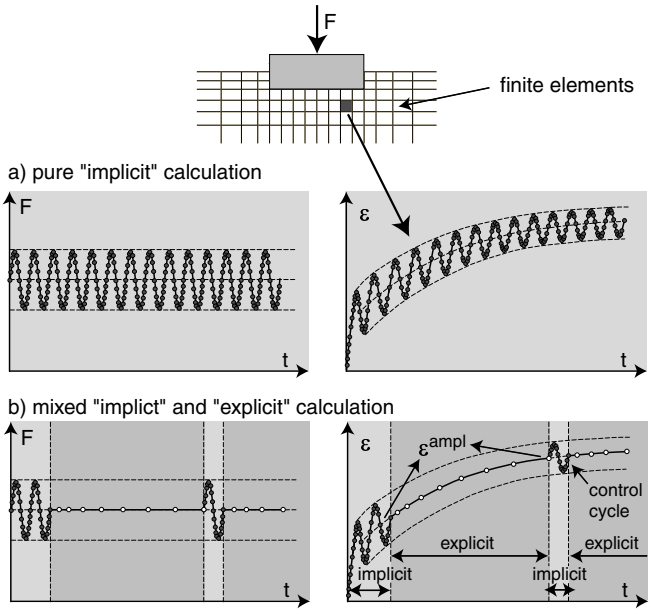

Fig. 1: Pure implicit versus combined implicit and explicit FE calculation of the settlement of a shallow foundation under cyclic loading

An important input parameter of the HCA model is the strain amplitude $\varepsilon^{\mathrm{ampl}}$ (Section 3). In order to determine the spatial field of the strain amplitude the implicit parts of the calculation are necessary. The first cycle may be *irregular* since the deformations in the first cycle can significantly differ from those in the subsequent cycles. The second cycle is more representative for the elastic portion of deformation during the subsequent cycles. Therefore, the strain amplitude is determined from the second cycle. For that purpose the strain path during the cycle is recorded in each integration point of the FE model. The strain amplitude is determined from the strain path according to the procedure described by Niemunis et al. [20]. During the explicit parts of the calculation the strain amplitude is assumed constant. During cyclic loading the spatial field of the strain amplitude may change due to compaction or a re-distribution of stress. Therefore, the explicit calculation should be interrupted after definite numbers of cycles (e.g. at $N = 10$, 100, 1000, etc.) and a so-called *control cycle* should be calculated implicitly in order to update the strain amplitude (Fig. 1b). The necessary number of control cycles depends on the boundary value problem and on the material under consideration.

3 High-cycle accumulation model

The HCA model proposed by Niemunis et al. [20] has been developed based on numerous drained cyclic triaxial and cyclic multiaxial DSS tests on sand (Wichtmann [33], Wichtmann et al. [34–36]). Deficits (lack of generality, missing influencing parameters, 1D formulation) of older HCA models proposed in the literature have been discussed in [33].

The strain and the stress path that result from a cyclic loading can be decomposed into an oscillating part (amplitude) and a trend (accumulation). The HCA model predicts the trends. The oscillating part is described by the strain amplitude. The basic equation of the HCA model reads

$$\dot{\boldsymbol{\sigma}} = \mathsf{E} : (\dot{\boldsymbol{\varepsilon}} - \dot{\boldsymbol{\varepsilon}}^{\mathrm{acc}} - \dot{\boldsymbol{\varepsilon}}^{\mathrm{pl}}) \tag{1}$$

The dot over a symbol means a derivative (rate) with respect to the number of cycles, that means

$$\dot{\sqcup} \;=\; \partial \sqcup / \partial N. \tag{2}$$

The colon in Eq. (1) means a double contraction (Gibbs notation). $\dot{\boldsymbol{\sigma}}$ is the trend of the effective stress $\boldsymbol{\sigma}$ (stress rate) and $\dot{\boldsymbol{\varepsilon}}$ is the trend of strain (strain rate). The sign convention of soil mechanics is used (i.e. compression positive). The HCA model prescribes the rate of strain accumulation $\dot{\boldsymbol{\varepsilon}}^{\mathrm{acc}}$. The plastic strain rate $\dot{\boldsymbol{\varepsilon}}^{\mathrm{pl}}$ is only necessary for stress paths touching the yield surface (see Niemunis et al. [20]). All stress and strain quantities in Eq. (1) are second-order tensors. E in Eq. (1) is a barotropic elastic stiffness (fourth-order tensor). Depending on the boundary conditions, the equilibrium iteration leads to a change of the average stress ($\dot{\boldsymbol{\sigma}} \neq 0$) and/or to an accumulation of residual strain ($\dot{\boldsymbol{\varepsilon}} \neq 0$).

For the presribed rate of strain accumulation in Eq. (1) the following expression is used:

$$\dot{\boldsymbol{\varepsilon}}^{\mathrm{acc}} \;=\; \dot{\varepsilon}^{\mathrm{acc}}\, \mathbf{m} \tag{3}$$

Therein the direction of strain accumulation ("cyclic flow rule")

$$\mathbf{m} \;=\; \dot{\boldsymbol{\varepsilon}}^{\mathrm{acc}} / \|\dot{\boldsymbol{\varepsilon}}^{\mathrm{acc}}\| \tag{4}$$

is a unit second-order tensor which describes the ratio between deviatoric and volumetric strain accumulation. The symbol $\| \sqcup \|$ means the Euclidean norm of a tensor. The scalar intensity of strain accumulation in Eq. (3) is

$$\dot{\varepsilon}^{\mathrm{acc}} \;=\; \|\dot{\boldsymbol{\varepsilon}}^{\mathrm{acc}}\|. \tag{5}$$

For sand it has been found experimentally [34] that the direction of strain accumulation primarily depends on the average stress ratio

$$\eta^{\mathrm{av}} = q^{\mathrm{av}} / p^{\mathrm{av}}. \tag{6}$$

The index $\sqcup^{\mathrm{av}}$ denotes the average value of $\sqcup$ during a cycle. For the triaxial case Roscoe's invariants (mean pressure p and deviatoric stress q) are defined as

$$p \;=\; (\sigma_1 + 2\sigma_3)/3 \qquad \text{and} \qquad q \;=\; \sigma_1 - \sigma_3 \tag{7}$$

with σ_1 and σ_3 being the axial and the lateral effective stress components, respectively. According to [34], cycles applied at an isotropic average stress ($\eta^{\mathrm{av}} = 0$) cause a

pure volumetric accumulation while a pure deviatoric accumulation takes place at an average stress ratio $\eta^{\mathrm{av}} = M_c$ or $\eta^{\mathrm{av}} = M_e$ corresponding to the critical state lines for triaxial compression or extension, respectively:

$$M_c = \frac{6\sin\varphi_c}{3-\sin\varphi_c} \qquad \text{and} \qquad M_e = -\frac{6\sin\varphi_c}{3+\sin\varphi_c} \tag{8}$$

with φ_c being the critical friction angle. It has been demonstrated in [34] that the direction of accumulation can be well approximated by the flow rule of the modified Cam clay (MCC) model:

$$\mathbf{m} = \left[\frac{1}{3}\left(p - \frac{q^2}{M^2 p}\right)\mathbf{1} + \frac{3}{M^2}\boldsymbol{\sigma}^*\right]^{\rightarrow} \tag{9}$$

The superposed arrow denotes an Euclidean normalization operator $\sqcup^{\rightarrow} = \sqcup / \| \sqcup \|$. The deviatoric part of stress is defined as

$$\boldsymbol{\sigma}^* = \boldsymbol{\sigma} - \frac{1}{3}\,\mathrm{tr}\,\boldsymbol{\sigma}\;\mathbf{1} \tag{10}$$

with $\mathrm{tr}\,\boldsymbol{\sigma}$ being the trace of the stress tensor and with an identity tensor $\mathbf{1}$. M in Eq. (9) is defined as

$$M = F\; M_c \tag{11}$$

with

$$F = \begin{cases} 1 + M_e/3 & \text{for } \eta \le M_e \\ 1 + \eta/3 & \text{for } M_e < \eta < 0 \\ 1 & \text{for } \eta \ge 0 \end{cases} \tag{12}$$

For the triaxial case Eq. (9) predicts strain rate ratios

$$\omega = \frac{\dot\varepsilon_v^{\mathrm{acc}}}{\dot\varepsilon_q^{\mathrm{acc}}} = \frac{M^2 - \eta^{\mathrm{av}2}}{2\eta^{\mathrm{av}}} \tag{13}$$

with $\dot\varepsilon_v^{\mathrm{acc}}$ and $\dot\varepsilon_q^{\mathrm{acc}}$ being the rates of volumetric and deviatoric strain accumulation, respectively, with Roscoe's invariants

$$\dot\varepsilon_v = \dot\varepsilon_1 + 2\dot\varepsilon_3 \qquad \text{and} \qquad \dot\varepsilon_q = \frac{2}{3}(\dot\varepsilon_1 - \dot\varepsilon_3) \tag{14}$$

Therein $\dot\varepsilon_1$ and $\dot\varepsilon_3$ are the rates of axial and lateral strain, respectively.

The intensity of strain accumulation $\dot\varepsilon^{\mathrm{acc}}$ in Eq. (3) is calculated as a product of six functions:

$$\dot\varepsilon^{\mathrm{acc}} = f_{\mathrm{ampl}}\; \dot f_N\; f_e\; f_p\; f_Y\; f_\pi \tag{15}$$

Each function (see Table 1) considers the influence of a different parameter.

The function f_{ampl} (see Table 1) describes the increase of the intensity of accumulation with increasing strain amplitude $\varepsilon^{\mathrm{ampl}}$. For various sands the exponent C_{ampl} (material constant) was found to be approx. 2.0 up to strain amplitudes of about 10^{-3} [37]. For larger strain amplitudes, the accumulation rate was observed to be almost independent of the strain amplitude [33].

The strain trajectories in a pavement due to a moving traffic load are multi-axial, that means they imply a rotation of the principal stress directions (Lekarp et al. [12]). The effect of the shape of the strain loop regarding the rate of strain accumulation has been confirmed experimentally (Pyke et al. [21], Wichtmann et al. [35]). It has been shown

Function	Const.	Sand	UGM
$f_{\mathrm{ampl}} = \left(\frac{\varepsilon^{\mathrm{ampl}}}{\varepsilon^{\mathrm{ampl}}_{\mathrm{ref}}}\right)^{C_{\mathrm{ampl}}} \le 100$	C_{ampl}	2.0	1.1
$f_e = \frac{(C_e - e)^2}{1+e}\;\frac{1+e_{\mathrm{ref}}}{(C_e - e_{\mathrm{ref}})^2}$	C_e	0.54	0.07
	e_{ref}	0.874	0.444
$f_p = \exp\left[-C_p\left(\frac{p^{\mathrm{av}}}{p_{\mathrm{ref}}} - 1\right)\right]$	C_p	0.43	-0.22
$f_Y = \exp\left(C_Y\,\bar Y^{\mathrm{av}}\right)$	C_Y	2.0	1.8
$\dot f_N = \dot f_N^A + \dot f_N^B$	C_{N1}	$3.6 \cdot 10^{-4}$	$5.2 \cdot 10^{-4}$
$\dot f_N^A = C_{N1}C_{N2}\exp\left[\frac{-g^A}{C_{N1} f_{\mathrm{ampl}}}\right]$	C_{N2}	0.43	0.03
$\dot f_N^B = C_{N1}C_{N3}$	C_{N3}	$5.0 \cdot 10^{-5}$	$1.3 \cdot 10^{-5}$

Table 1: Summary of the functions and the material constants of the HCA model ($p_{\mathrm{ref}} = 100$ kPa, $\varepsilon^{\mathrm{ampl}}_{\mathrm{ref}} = 10^{-4}$, $e_{\mathrm{ref}} = e_{\max}$)

that circular strain loops produce twice larger accumulation rates than one-dimensional cycles. The HCA model incorporates a tensorial definition of the amplitude for such multi-axial strain loops [20]. The present paper discusses only laboratory tests with uniaxial cycles. In that case the novel amplitude definition is equal to the conventional one, that means

$$\sqcup^{\mathrm{ampl}} = \frac{1}{2}(\sqcup^{\max} - \sqcup^{\min}). \tag{16}$$

The function f_e in Eq. (15) (see Table 1) with its material constant C_e describes the increase of the rate of strain accumulation with increasing void ratio e.

For a constant average stress ratio η^{av}, the intensity of strain accumulation increases with decreasing average mean pressure p^{av}. For a constant average mean pressure, the permanent strain accumulation increases with increasing average stress ratio. These dependencies were observed for various sands [37]. They are captured by the exponential functions f_p and f_Y with material constants C_p and C_Y, respectively (see Table 1). In the function f_Y the stress ratio is described by $\bar Y^{\mathrm{av}}$ instead of η^{av}, using the function Y of Matsuoka & Nakai [16]:

$$\bar Y = \frac{Y-9}{Y_c - 9} \quad \text{with} \quad Y_c = \frac{9 - \sin^2\varphi_c}{1 - \sin^2\varphi_c} \quad \text{and} \tag{17}$$

$$Y = \frac{27(3+\eta)}{(3+2\eta)(3-\eta)} \tag{18}$$

The stress ratio $\bar Y^{\mathrm{av}}$ is zero at an isotropic average stress and equal to one on the critical state lines.

The increase of the permanent strain $\varepsilon^{\mathrm{acc}}$ with increasing number of cycles runs proportional to the function f_N of the HCA model:

$$\varepsilon^{\mathrm{acc}}(N) \sim f_N = C_{N1}\left[\ln(1 + C_{N2}N) + C_{N3}N\right] \tag{19}$$

with material constants C_{N1}, C_{N2} and C_{N3}. Its derivative with respect to N reads

$$\dot f_N = \underbrace{\frac{C_{N1}C_{N2}}{1 + C_{N2}N}}_{\dot f_N^A} + \underbrace{C_{N1}C_{N3}}_{\dot f_N^B} \tag{20}$$

It can be splitted into a N-dependent portion $\dot{f}_N^A$ and a constant portion $\dot{f}_N^B$. The number of cycles alone is not a suitable state variable for the quantification of cyclic preloading (historiotropy) since it contains no information about the amplitude of the cycles in the past. For that reason, the preloading (historiotropic) variable g^A was introduced into the HCA model. It counts the cycles weighting them with their amplitude

$$g^A = \int f_{\mathrm{ampl}} \, \dot{f}_N^A \, \mathrm{d}N \tag{21}$$

Only the N-dependent portion of $\dot{f}_N$ is considered for g^A. The function $\dot{f}_N^A$ was re-formulated using g^A instead of N (see Table 1). The HCA model with its historiotropic variable g^A is able to predict the accumulation of strain due to packages of cycles with different amplitudes applied in different sequences. The model approximately obeys Miner's rule [17] known from fatigue mechanics of metals, that means the sequence of the packages of cycles is of no importance, which is in good accordance with the experiments presented by Kaggwa et al. [11] and Wichtmann [33].

The factor f_π in Eq. (15) considers that a change of the polarization (direction) of the cycles leads to a temporary increase of the rate of accumulation (Wichtmann et al. [35], Yamada & Ishihara [39]). A detailed description of this factor can be found in [20]. Due to the constant polarization of the cycles $f_\pi = 1$ holds for the triaxial tests presented herein.

Since the accumulation of residual strain does not depend on the loading frequency (Youd [40], Shenton [26], Wichtmann et al. [34], Duku et al. [6]), the loading frequency is not a parameter of the HCA model.

4 Description of the tests

4.1 Tested materials

The grain size distribution curves and the index properties of the tested materials are shown in Fig. 2. The tested sand is medium coarse to coarse and rather uniform. The grain size distribution curve of the UGM is in accordance with the Colombian Specification [5] for base layer construction in flexible pavements except for the maximum grain size. It was reduced to $d_{\max} = 16$ mm in order not to fall below a ratio $b/d_{\max}$ of 5 with $b \times b$ being the dimensions of the specimen cross section in the triaxial tests. Both grain size distribution curves were mixed from a natural quartz sand with subangular grains and a specific weight of $\varrho_s = 2.65$ g/cm^3. In the case of the UGM a quartz meal was used for the fine particles. The minimum and maximum void ratios given in Fig. 2 were determined according to German standard code DIN 18126 [1].

4.2 Test device and specimen preparation

A scheme of the used triaxial device has been shown by Rondón et al. [23]. For the tests on sand cylindrical specimens with a diameter $d = 10$ cm and a height $h = 20$ cm were used. The UGM specimens were prismatic with dimensions $8.7 \times 8.7 \times 18$ cm. The square cross section was chosen because it is advantageous for local measurements of the lateral strain by means of so-called LDTs (Goto et al. [8]). Lubricated end plates equipped with a thin rubber membrane and with small central porous stones were used. The tests were performed drained and stress-controlled.

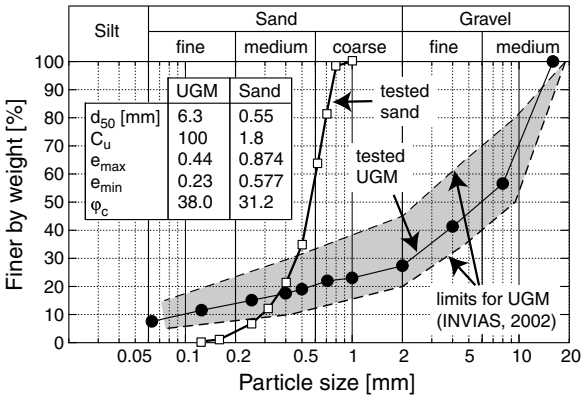

Fig. 2: Grain size distribution curves and index properties of the tested materials

The cyclic axial load was applied with a pneumatic loading system.

The axial load was measured inside the pressure cell with a load cell located below the bottom end plate. The axial deformation was obtained from a displacement transducer attached to the load piston. The system compliance was determined in preliminary tests on a steel dummy and was subtracted from the measured displacement. In [23] it has been demonstrated that the axial strain determined in that way is in good agreement with the axial strain measured locally in the middle of the specimen by means of LDTs. For that reason, local measurements were left out in the present study. Volume changes were measured via the pore water of the fully saturated specimens using a pipette system and a differential pressure transducer. The data were recorded during the first 25 cycles and during five cycles at $N = 50$, 100, 200, 500, ..., $5 \cdot 10^4$ and 10^5.

The sand specimens were prepared by pluviating dry sand out of a funnel into split moulds. The UGM specimens were prepared by moist tamping in six layers. The material was placed with the optimum water content ($w_{\mathrm{opt}} = 5.2$ %, $\varrho_{\mathrm{Pr}} = 2.30$ g/cm^3) determined in a Proctor test with modified energy. A miniature proctor hammer was used for compaction of the specimens. Its fall weight ($m = 1$ kg) was dropped from a height of $H = 20$ cm. $N = 250$ blows were applied to each layer. The induced energy was chosen lower than that used in the modified Proctor test in order to reach densities in the range of 93 - 96 % of ϱ_{Pr}, which are typical for UGM layers in situ. All UGM specimens were compacted using the same energy (except those for the tests on the density-influence) in order to induce the same initial fabric. The large influence of the initial fabric on the rate of strain accumulation has been demonstrated for example by Triantafyllidis et al. [29]. In order to measure volume changes via the pore water, both, the sand and the UGM specimens were first flushed with CO_2 and then saturated with de-aired water. A back pressure of 200 kPa was used in all tests. The saturation was controlled by Skempton's B-Value. In all tests $B > 0.95$ was achieved.

4.3 Testing program

For both the sand and the UGM four test series were performed. Throughout the tests of each series a single parameter (stress amplitude q^{ampl}, initial void ratio e_0, average

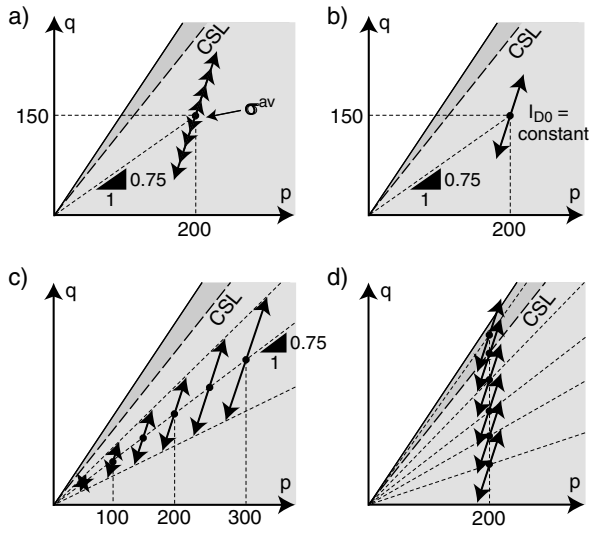

Fig. 3: Effective stress cycles in the four series of cyclic triaxial tests performed on each material

mean pressure p^{av} or average stress ratio η^{av}) was varied while the remaining were kept constant. The effective stress paths are shown schematically in the p-q-plane in Fig. 3. For each stress path, a new specimen was prepared, that means no multi-stage tests were performed. In the first series of tests (Fig. 3a) the stress amplitude was varied at a constant average stress ($p^{\mathrm{av}} = 200$ kPa, $\eta^{\mathrm{av}} = 0.75$). In the second series of tests (Fig. 3b) the initial density was varied. It is described by the density index

$$I_{D0} = (e_{\max} - e_0)/(e_{\max} - e_{\min}) \quad (22)$$

or by the percentage of the Proctor density. The tests on the influence of density were performed at the same average stress ($p^{\mathrm{av}} = 200$ kPa, $\eta^{\mathrm{av}} = 0.75$). In the third series (Fig. 3c) different average mean pressures between 50 kPa and 300 kPa were tested while the average stress ratio was kept constant at $\eta^{\mathrm{av}} = 0.75$. The amplitude-pressure ratio

$$\zeta = q^{\mathrm{ampl}}/p^{\mathrm{av}} \quad (23)$$

was also kept constant within the series. The fourth series of tests was performed with constant values of average mean pressure ($p^{\mathrm{av}} = 200$ kPa) and stress amplitude but with different average stress ratios (Fig. 3d).

The average and cyclic stresses were chosen in accordance with our recommendations for the determination of the material constants of the HCA model (Wichtmann et al. [38]). In most experimental studies on permanent deformations in pavements, cycles with an isotropic minimum stress ($q^{\min} = 0$) were applied, which is a special case of the tests shown in Fig. 3d. Such stress paths are also recommended by the standard code EN 13286-7 [2]. Since the HCA model is formulated for general stress states, the stress cycles chosen for the calibration of the material constants are more general than those usually tested in pavement engineering.

Furthermore, in comparison with other studies on UGM in the literature and in comparison to the recommendations in EN 13286-7 [2], the stress and strain amplitudes applied in the present study are relatively low. This is due to the fact that in typical applications of the HCA model (e.g. tilting of on-shore and off-shore wind power plants, settlement of railways of high-speed trains) the strain amplitudes usually do not exceed 10^{-3}. The present study focusses on the application of the HCA model to UGM and on a comparison of sand and UGM behavior under cyclic loading. For that purpose similar stress and strain amplitudes as usually used for sand were also chosen for the tests on the UGM.

After the application of the average stress and a resting period of 1 hour, the cyclic loading was commenced. Due to the larger deformations and in order to prevent a build-up of excess pore water pressure, the first *irregular* cycle was applied with a low frequency of one cycle per 100 seconds ($f = 10$ mHz). Subsequently, 100,000 *regular* cycles with a frequency $f = 1$ Hz were applied in all tests.

5 Test results

From the measured vertical displacement and volume change the axial strain ε_1 and the volumetric strain ε_v were calculated. The lateral strain ε_3 and the deviatoric strain ε_q were obtained from Eq. (14). From the minimum and maximum values during a cycle the residual portion (denoted by $\sqcup^{\mathrm{acc}}$) and the resilient portion (denoted by $\sqcup^{\mathrm{ampl}}$) of the strain components were determined. The strain amplitude and the residual strain are

$$\varepsilon^{\mathrm{ampl}} = \sqrt{(\varepsilon_1^{\mathrm{ampl}})^2 + 2(\varepsilon_3^{\mathrm{ampl}})^2} \quad \text{and} \quad (24)$$

$$\varepsilon^{\mathrm{acc}} = \sqrt{(\varepsilon_1^{\mathrm{acc}})^2 + 2(\varepsilon_3^{\mathrm{acc}})^2} \quad (25)$$

5.1 Influence of the amplitude

While for the sand eight tests with stress amplitudes 12 kPa $\leq q^{\mathrm{ampl}} \leq$ 80 kPa were performed, the three amplitudes $q^{\mathrm{ampl}} = 30$, 60 and 90 kPa were tested for the UGM.

For sand the strain amplitude $\varepsilon^{\mathrm{ampl}}$ decreases during the first 100 cycles and stays almost constant afterwards [33]. For the UGM a continuous increase of the strain amplitude during the first 20,000 cycles and approximately constant values for larger numbers of cycles were observed. Since the tests were performed drained and a constant pore water pressure was measured, the increase of the strain amplitude cannot be attributed to a build-up of pore water pressure.

If a mean value of the strain amplitude over 10^5 cycles is plotted versus the stress amplitude, almost linear curves are obtained for sand. For UGM the strain amplitude increases faster than linear with the stress amplitude. For both materials, the average values of the strain amplitude lay in the range between $5 \cdot 10^{-5}$ and $4 \cdot 10^{-4}$.

Figure 4a contains the curves of the residual strain $\varepsilon^{\mathrm{acc}}$ as a function of the number of cycles. For the sand the strain increases proportional to the logarithm of N up to $N \approx 10^4$ and faster for larger number of cycles. For the UGM the curves are overlogarithmic between $N = 1$ and $N = 10^4$ and run almost proportional to $\ln(N)$ for larger numbers of cycles. Therefore, the curves $\varepsilon^{\mathrm{acc}}(N)$ measured for UGM are similar to those obtained for air-pluviated specimens of well-graded sands [37].

As obvious from Figure 4a, for both materials the permanent strain increases with increasing stress amplitude. This is in agreement with test results in the literature (e.g. Youd [40], Silver & Seed [27, 28], Sawicki & Świdziński [24, 25], Marr & Christian [15], Duku et al. [6]). In Figure 4b the residual strain is given as a function of the strain amplitude

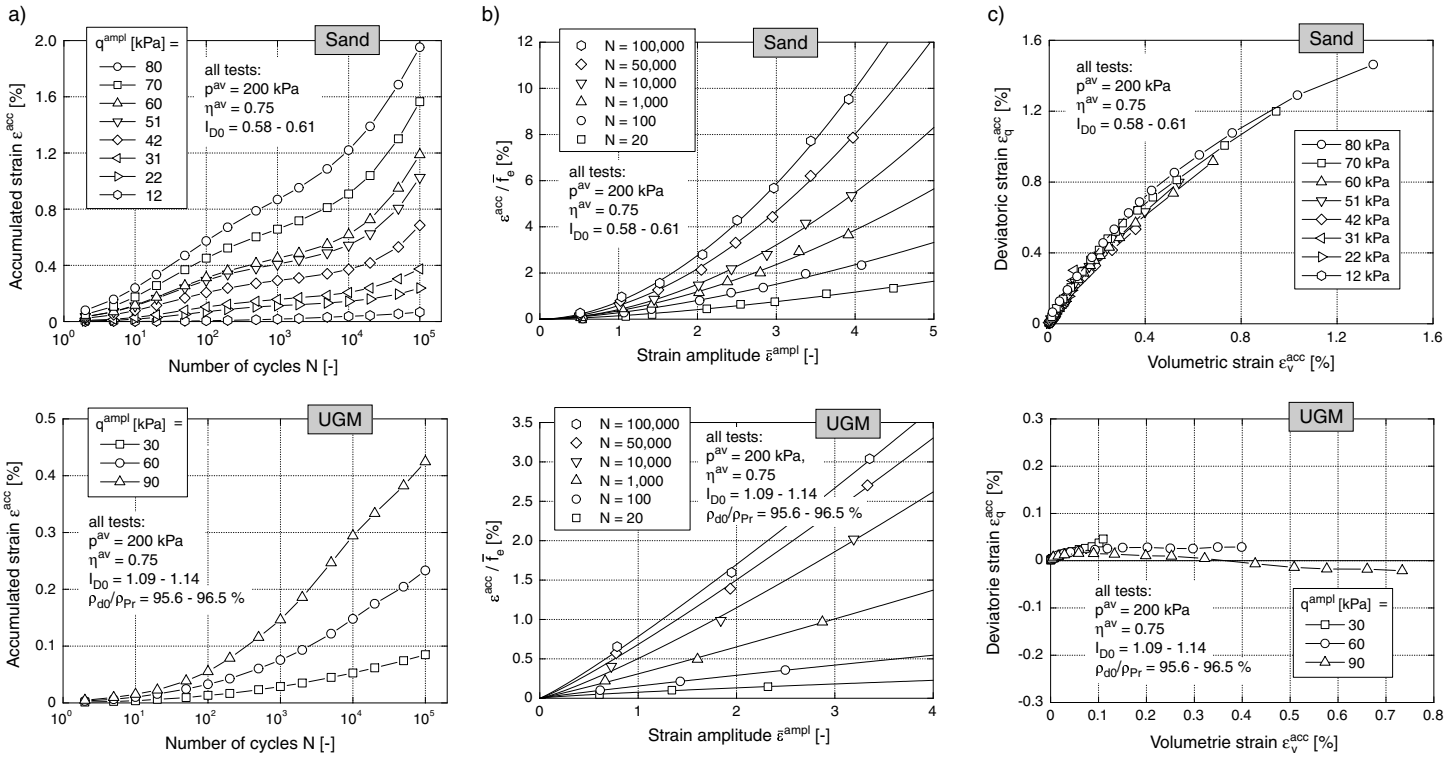

Fig. 4: *Tests with different stress amplitudes q^{ampl}: a) Accumulation curves $\varepsilon^{acc}(N)$, b) Permanent strain (divided by the void ratio function) $\varepsilon^{acc}/\bar{f}_e$ versus strain amplitude $\bar{\varepsilon}^{ampl}$, c) ε_v^{acc}-ε_q^{acc} strain paths*

$\bar{\varepsilon}^{\mathrm{ampl}}$. The bar over a symbol indicates that a mean value up to the number of cycles N has been used:

$$\square^{\mathrm{ampl}} \;=\; 1/N \int \sqcup^{\mathrm{ampl}}(N)\; \mathrm{d}N. \tag{26}$$

On the ordinate the permanent strain has been divided by the void ratio function $\bar{f}_e$ (Table 1) which considers the different initial void ratios e_0 and different compaction rates $\dot{e}$. The bar over f_e indicates that a mean value $\bar{e}$ is used when calculating the void ratio function. The function f_{ampl} developed for sand is also suitable to describe the amplitude-dependence for the UGM. However, the exponent C_{ampl} is significantly different for both materials. A curve-fitting of

$$f \;=\; c\,(\bar{\varepsilon}^{\mathrm{ampl}})^{C_{\mathrm{ampl}}} \tag{27}$$

to the data in Figure 4b (the constant c is not used further) delivered mean values of C^{ampl} of approximately 2.0 for sand but only 1.1 for the UGM. Therefore, the proportionality between the accumulation rate and the square of the strain amplitude which was observed for various sands does not apply to the pre-compacted UGM samples.

Figure 4c presents the permanent deviatoric strain $\varepsilon_q^{\mathrm{acc}}$ as a function of the permanent volumetric strain $\varepsilon_v^{\mathrm{acc}}$. The data points correspond to numbers of cycles N = 2, 5, 10, 20, 50, 100, ... 10^5. For sand and for UGM the direction of the $\varepsilon_v^{\mathrm{acc}}$-$\varepsilon_q^{\mathrm{acc}}$-strain paths and therefore the direction of accumulation $\mathbf{m}$ in the HCA model does not significantly depend on the amplitude. However, the directions are different for sand and for UGM which will be further discussed in Section 5.4.

5.2 Influence of void ratio / density

For the sand nine tests with different initial relative densities in the range $0.54 \le I_{D0} \le 0.99$ were performed. The initial relative densities in the tests on the UGM lay in the range $0.71 \le I_{D0} \le 1.09$ which corresponds to dry densities between 89.4 % and 95.7 % of the Proctor density. The three specimens with the lower densities were prepared using a reduced number of blows per layer (50, 100 or 150, respectively).

In accordance with earlier test results (Silver & Seed [27, 28], Youd [40], Hain [9], Marr & Christian [15], Duku et al. [6]) the accumulation rate increases with decreasing density for both materials (Figure 5a). Figure 5b presents the residual strain as a function of a mean value of the void ratio. In order to consider the slight increase of the strain amplitude with decreasing density, the residual strain has been divided by the amplitude function $\bar{f}_{\mathrm{ampl}}$ of the HCA model. It was calculated with a mean value $\bar{\varepsilon}^{\mathrm{ampl}}$ of the strain amplitude and with constants $C_{\mathrm{ampl}} = 2.0$ for sand and $C_{\mathrm{ampl}} = 1.1$ for UGM. For both materials the void-ratio-dependence of the accumulation rate can be described by the same function f_e. A fitting of

$$f = c\,\frac{(C_e - e)^2}{(1+e)} \tag{28}$$

to the data in Figure 5b resulted in material constants C_e = 0.54 for sand and C_e = 0.07 for UGM.

For sand the direction of accumulation does not depend on the density (Figure 5c). For UGM the test results are somewhat ambiguous. Neglecting the test with a density index I_{D0} = 0.86 there is a tendency that the accumulation becomes more deviatoric with decreasing density, that means with decreasing number of blows during specimen

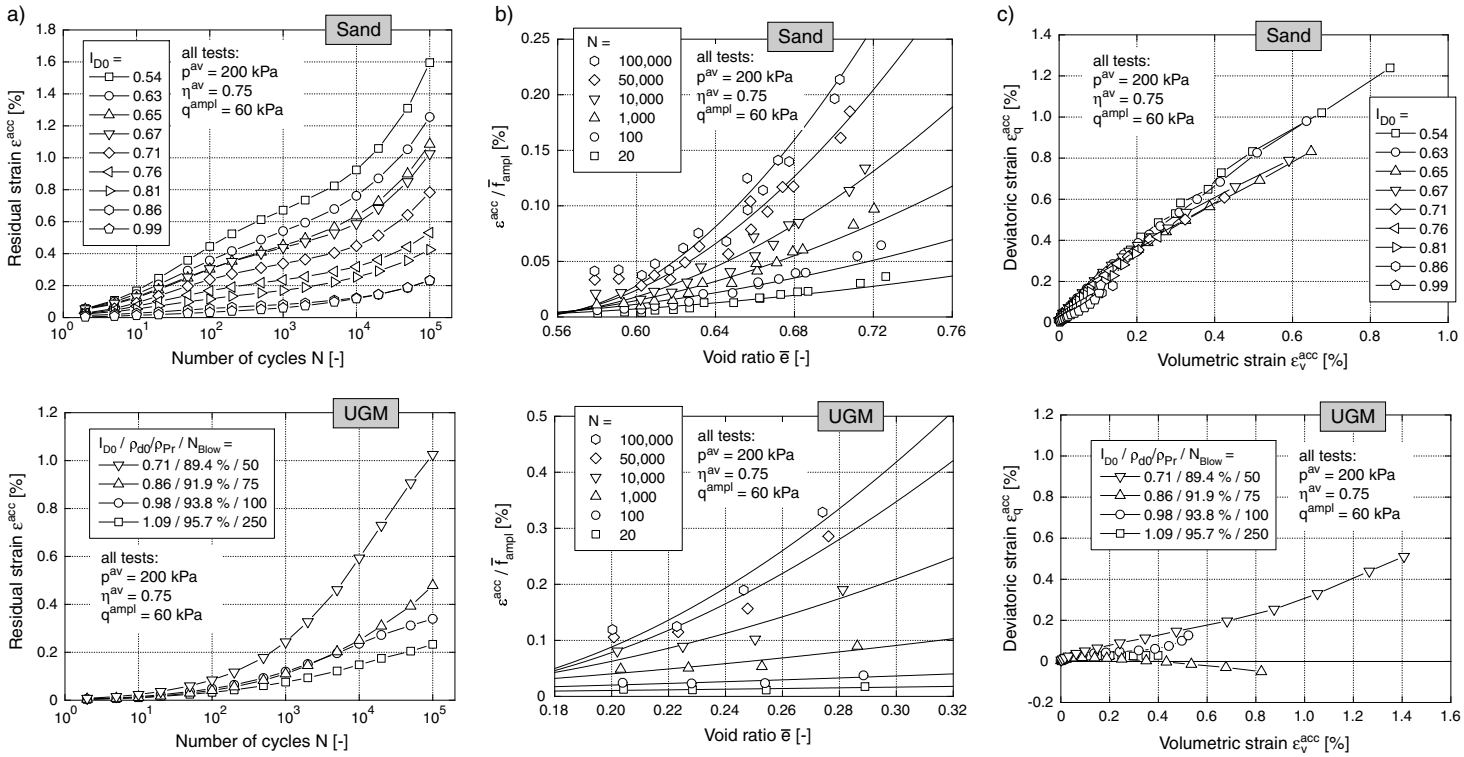

Fig. 5: *Tests with different initial densities: a) Accumulation curves $\varepsilon^{acc}(N)$, b) Permanent strain (divided by the amplitude function) $\varepsilon^{acc}/\bar{f}_{ampl}$ versus void ratio $\bar{e}$, c) ε_v^{acc}-ε_q^{acc} strain paths*

preparation. However, although looser than the samples with $I_{D0} = 0.98$ and 1.09, the specimen with $I_{D0} = 0.86$ shows a less deviatoric accumulation. A possible density-dependence of the direction of accumulation for the UGM needs further investigations. It is neglected in the HCA model for the moment.

5.3 Influence of average mean pressure

For the sand six tests and for the UGM four tests with different average mean pressures in the range 50 kPa $\leq p^{av} \leq$ 300 kPa were performed. An average stress ratio of $\eta^{av} = 0.75$ and an amplitude ratio of $\zeta = 0.3$ were chosen for both materials. Due to the constant amplitude ratio, the strain amplitudes increase with increasing average mean pressure.

For sand the curves $\varepsilon^{acc}(N)$ for different average mean pressures coincide for low numbers of cycles ($N < 10^4$) and diverge at larger N-values (Figure 6a). The accumulation rates increase with decreasing average mean pressure. This is in accordance with simple shear test results of Duku et al. [6]. For the UGM the curves $\varepsilon^{acc}(N)$ for different pressures diverge from the beginning of the tests. Opposite to the observations for sand, in the tests on UGM the largest residual strain was obtained for the largest pressure while the smallest one was observed for the smallest pressure.

The opposite p^{av}-dependence for sand and for UGM becomes also clear from Figure 6b where the residual strain has been divided by the amplitude and by the void ratio function of the HCA model in order to free the data from the influences of strain amplitude and void ratio. The data is plotted versus the average mean pressure. Although the pressure-dependence is opposite, the barotropy function f_p developed for sand can also be used for the UGM. For UGM the parameter C_p is negative. The function

$$f = c \ \exp\left[-C_p \ (p^{av}/100 - 1)\right] \tag{29}$$

has been fitted to the data in Fig. 6b in order to determine C_p. For sand C_p increases from 0.25 for $N = 20$ to 0.66 for $N = 10^5$ (see remarks in [34]). A mean value $C_p = 0.43$ is used in the following. Such an N-dependence was not observed for the UGM, where an almost constant value of $C_p = -0.22$ was found.

Although the directions of the strain paths are different for sand and for UGM (Figure 6c), for both materials the direction does not significantly depend on the average mean pressure.

5.4 Influence of average stress ratio

For sand eleven tests with different average stress ratios in the range $0.25 \leq \eta^{av} \leq 1.313$ were performed. For UGM the influence of the stress ratio was studied in four tests with $0.25 \leq \eta^{av} \leq 1.5$. The average mean pressure was p^{av} = 200 kPa and the stress amplitude was $q^{ampl} = 60$ kPa in all tests.

For sand and for UGM the strain amplitude decreases with increasing average stress ratio. Obviously, for both materials the accumulation rate increases with increasing stress ratio (Figure 7a). This becomes also clear from Figure 7b in which the accumulated strain has been normalized with the amplitude and the void ratio function of the HCA model and plotted versus the stress ratio $\bar{Y}^{av}$. For both materials the stress-ratio-dependence can be described by the same function f_Y. A curve-fitting of

$$f = c \ \exp(C_Y \bar{Y}^{av}) \tag{30}$$

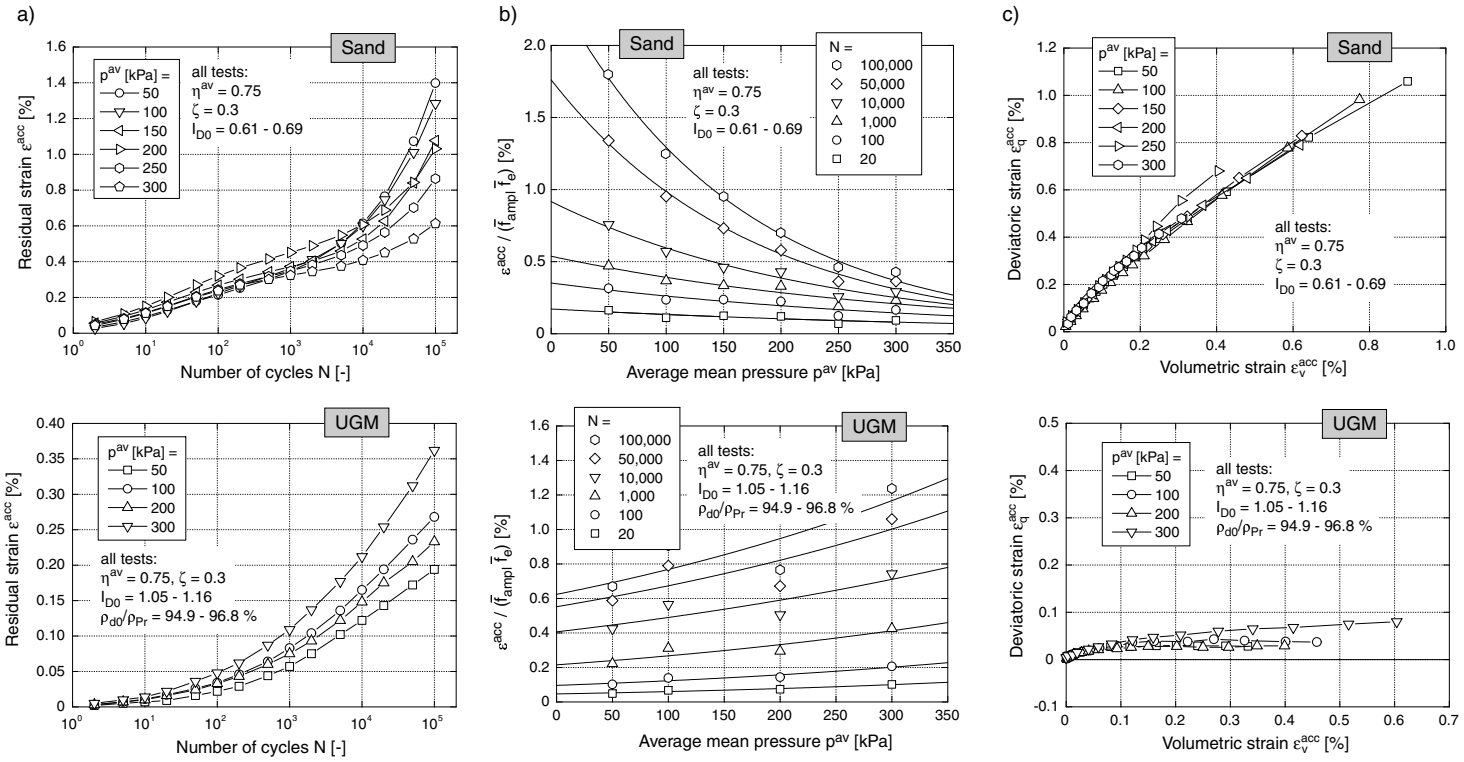

Fig. 6: *Tests with different average mean pressures p^{av}: a) Accumulation curves $\varepsilon^{acc}(N)$, b) Permanent strain (divided by the amplitude and void ratio functions) $\varepsilon^{acc}/(\bar{f}_{ampl}\bar{f}_e)$ as a function of average mean pressure p^{av} c) ε_v^{acc}-ε_q^{acc} strain paths*

to the data in Fig. 7b resulted in similar mean values of the material constant C_Y (2.0 for sand and 1.8 for UGM). Only a slight variation of C_Y with the number of cycles was observed for both materials.

Figure 7c presents the $\varepsilon_v^{\mathrm{acc}}$-$\varepsilon_q^{\mathrm{acc}}$ strain paths for different average stress ratios. For sand, the accumulation is pure volumetric ($\dot{\varepsilon}_q^{\mathrm{acc}} \approx 0$) if the cycles are applied at an isotropic average stress ($\eta^{\mathrm{av}} = 0$). The accumulation becomes more deviatoric with increasing average stress ratio. A pure deviatoric accumulation ($\dot{\varepsilon}_v^{\mathrm{acc}} \approx 0$) takes place at an average stress lying on the critical state line (CSL, determined from monotonic shear tests). While for an average stress below the CSL the cycles cause compaction, a dilative accumulation is observed above the CSL. The test results are in good accordance with earlier works of Luong [14] and Chang & Whitman [4].

For UGM, an increase of the deviatoric portion of accumulation with increasing average stress ratio was also observed. However, compared to the tests on sand, the accumulation is pure volumetric at a much larger stress ratio $\eta^{\mathrm{av}} \approx 0.5$. For a stress ratio $\eta^{\mathrm{av}} = 0.25$ negative rates of deviatoric strain accumulation were observed. In contrast to the results for sand, the rate of volumetric strain accumulation did not vanish at a stress ratio $\eta^{\mathrm{av}} = 1.5$ which is near to the stress ratio $M_c = 1.55$ corresponding to the critical state line. It should be mentioned that the critical friction angle $\varphi_c = 38°$ given in Figure 2 was determined from the inclination of a cone of dry material loosely deposited by lifting a funnel. This φ_c-value may not be representative for the pre-compacted UGM samples. Monotonic triaxial tests on the UGM (Rondon et al. [23]) indicated larger residual stress ratios $M_c \approx 1.8$ at large strains, corresponding to a friction angle $\varphi_c \approx 44°$. Possibly, the accumulation becomes pure deviatoric at a stress ratio $\eta^{\mathrm{av}} \approx 1.8$. In that case the assumption of a pure deviatoric accumulation at a stress ratio $\eta^{\mathrm{av}} = M_c$ can be maintained for the UGM.

We distinguish between an *inherent* and an *induced* anisotropy. The observed anisotropy of the UGM samples has been induced during the preparation procedure due to compaction. An inherent anisotropy may be due to the grain characteristics, for example caused by flat or elongated grains. Since an isotropic direction of accumulation has been observed for sand, there is no inherent anisotropy for the studied sub-angular grain shape.

The isotropic flow rule $\mathbf{m}$ used for sand turns out to be insufficient for the UGM. The test results in the lower diagram of Fig. 7c can hardly be reproduced with an isotropic flow rule. Therefore, for an application of the HCA model to the UGM the flow rule has to be generalized in order to describe anisotropy. This generalization is discussed in the following. The equations do not distinguish between an inherent and an induced anisotropy. For that purpose a second-order anisotropy tensor

$$\mathbf{a} \quad = \quad \boldsymbol{\sigma}^*/p \tag{31}$$

is introduced with $\boldsymbol{\sigma}$ being a stress for which the flow rule is assumed purely volumetric, $\mathbf{m}(\mathbf{a}) = \vec{\mathbf{1}}$. The isotropic flow rule can be recovered by setting $\mathbf{a} = \mathbf{0}$. For the critical state the flow rule is purely deviatoric. For an intermediate stress $\boldsymbol{\sigma}$ an interpolation is used. Given $\mathbf{a}$, the stress $\boldsymbol{\sigma}$ is projected radially onto the deviatoric plane expressed by $p = 1$. Next, the projected stress $\boldsymbol{\sigma}$/p is decomposed as follows (Figure 8a):

$$\boldsymbol{\sigma}/p \quad = \quad \mathbf{1} + \mathbf{r} \;=\; \mathbf{1} + \boldsymbol{\sigma}^*/p \tag{32}$$

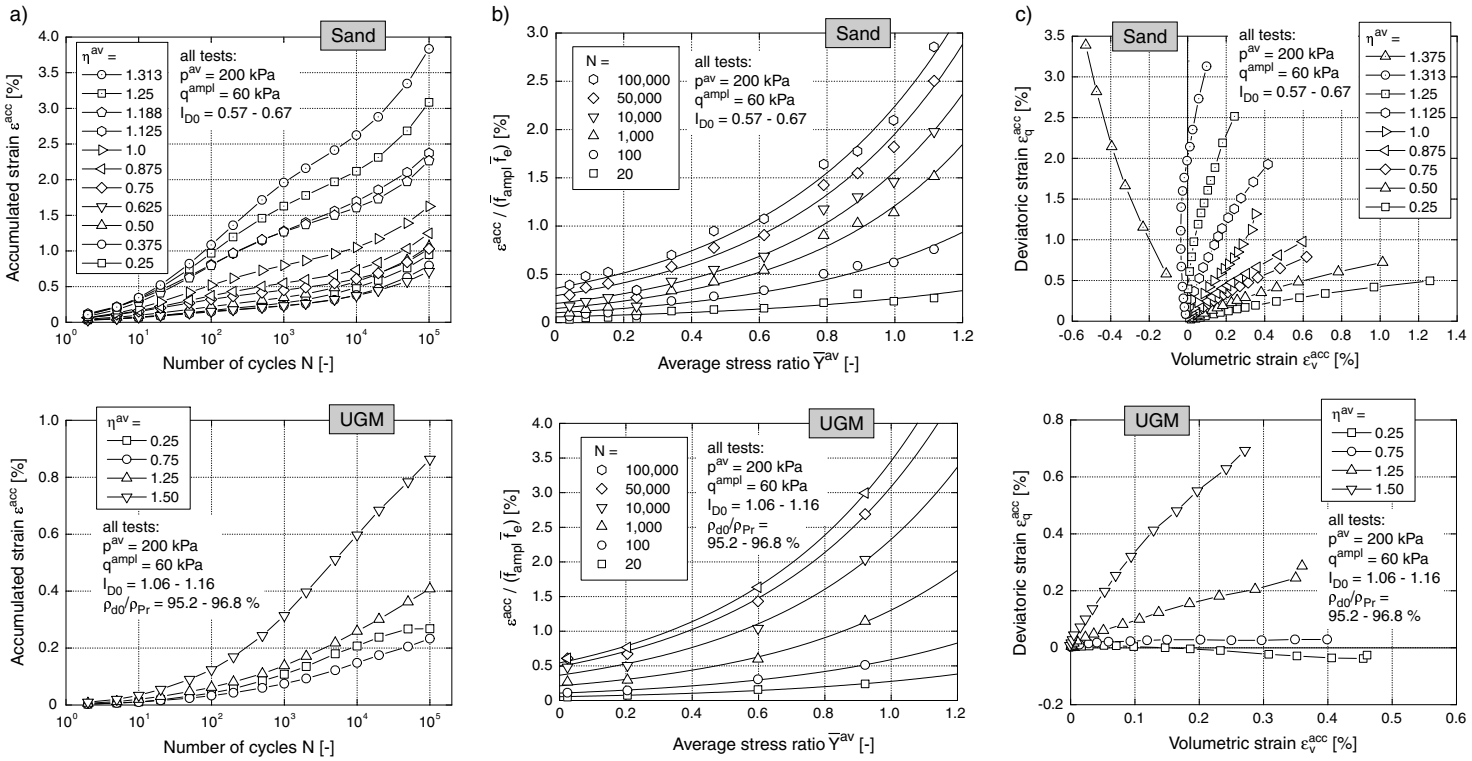

Fig. 7: *Tests with different average stress ratios η^{av}: a) Accumulation curves $\varepsilon^{acc}(N)$, b) Permanent strain (divided by the amplitude and void ratio functions) $\varepsilon^{acc}/(\bar{f}_{ampl}\bar{f}_e)$ versus normalized average stress ratio $\bar{Y}^{av}$ c) ε_v^{acc}-ε_q^{acc} strain paths*

The so-called conjugated stress $\mathbf{t}$ is found from

$$\mathbf{t} \;=\; \mathbf{1} + \mathbf{a} + \lambda(\mathbf{r} - \mathbf{a}) \tag{33}$$

It should lie on the critical surface at $p = 1$ (Figure 8b). For that purpose the scalar multiplier λ must be determined from the condition that the conjugated stress $\mathbf{t}$ satisfies

$$\mathrm{tr}\,\mathbf{t}\;\mathrm{tr}\,(\mathbf{t}^{-1}) = Y_c \qquad \text{or} \qquad \mathrm{tr}\,(\mathbf{t}^{-1}) = -Y_c/3 \tag{34}$$

with Y_c calculated from Eq. (17). Having found λ the generalized flow rule is calculated from

$$\mathbf{m} = \frac{1}{\sqrt{(1-\lambda^{-n})^2 + (\lambda^{-n})^2}} \left[\vec{\mathbf{1}}(1-\lambda^{-n}) + \lambda^{-n}(\mathbf{t}^*)^{\rightarrow}\right] \tag{35}$$

wherein n is an interpolation parameter (a material constant). Linear interpolation is obtained with $n = 1$.

As an example, the flow rule $\mathbf{m}$ for an axisymmetric stress with diagonal components

$$\boldsymbol{\sigma} \;=\; \mathrm{diag}(\sigma_1, \sigma_3, \sigma_3) \tag{36}$$

and for a transversal isotropy

$$\mathbf{a} \;=\; \mathrm{diag}(a, -a/2, -a/2). \tag{37}$$

is derived. The parameter a and the stress ratio η_{iso} for which the accumulation is purely volumetric are interrelated via

$$a \;=\; -2/3\;\eta_{\mathrm{iso}}. \tag{38}$$

Furthermore,

$$\mathbf{r} \;=\; \mathrm{diag}(r, -r/2, -r/2) \quad \text{with} \quad r = -2/3\;\eta \tag{39}$$

holds. From two solutions of Eq. (34)

$$\lambda_{1|2} = \frac{1}{2(a-r)^2 Y_c}\Big[-9a + 3\left(3r \pm \sqrt{(a-r)^2(Y_c-9)(Y_c-1)}\right) + (2a+1)(a-r)Y_c\Big] \tag{40}$$

the positive one is chosen as λ. Finally, the strain rate ratio ω is calculated from

$$\omega \;=\; \frac{1-\lambda^{-n}}{\lambda^{-n}} \quad \text{or} \quad \omega \;=\; -\,\frac{1-\lambda^{-n}}{\lambda^{-n}} \tag{41}$$

for triaxial compression and extension, respectively. In Figure 8c curves $\omega(\eta^{\mathrm{av}})$ predicted either by Eq. (13) or by Eq. (41) are compared for a critical friction angle of $\varphi_c = 30°$ and for an isotropic material ($\eta_{\mathrm{iso}} = 0$). Using an interpolation constant $n = 0.9$ in Eq. (41), both curves coincide well, except some diverging in the over-critical regime.

In Fig. 8d,e the direction of strain accumulation is shown by vectors in the p-q-plane. The vectors start at the average stress of a test and have an inclination of $\varepsilon_q^{\mathrm{acc}}/\varepsilon_v^{\mathrm{acc}}$ towards the horizontal. The increase of the volumetric portion of accumulation with the number of cycles, that means the decrease of the inclination of the vectors is more pronounced for the UGM. For sake of simplicity the dependence of $\mathbf{m}$ on the number of cycles has not been implemented into the HCA model yet. The test data are compared with the predictions by Eqs. (13) and (41), respectively. For sand, the direction of accumulation is well approximated by the isotropic MCC flow rule (Fig. 8d). For $\eta_{\mathrm{iso}} = 0$ and $n = 0.9$ the flow rule defined by Eq. (41) delivers similar vectors in the p-q-plane (at least in the under-critical regime, Fig. 8d). The vectors in Fig. 8e were generated using Eq. (41) with $\eta_{\mathrm{iso}} = 0.5$, $\varphi_c = 44°$ and $n = 0.9$. They reproduce well the experimentally obtained vectors, especially for larger numbers of cycles $N > 10^4$.

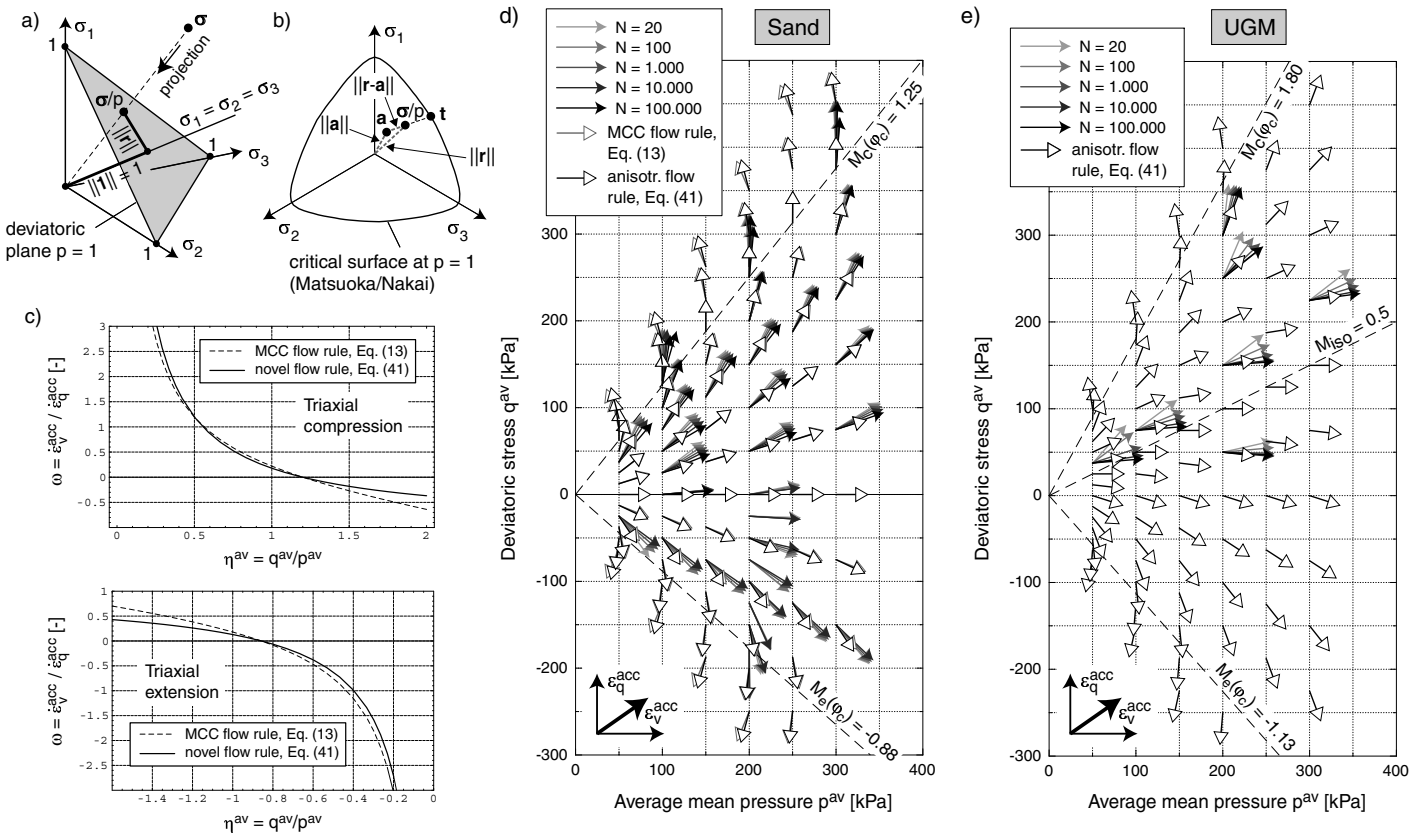

Fig. 8: *a) Projection of stress* $\boldsymbol{\sigma}$ *on the surface* $p = 1$*, b) Determination of the conjugated stress* $\mathbf{t}$*, c) Comparison of curves* $\omega(\eta^{av})$ *for* $\varphi_c = 30°$*,* $\eta_{iso} = 0$ *and* $n = 0.9$*, d),e)* $\mathbf{m}$ *shown as vectors in the p-q-plane*

5.5 Influence of the number of cycles

In Figure 9 all curves $\varepsilon^{acc}(N)$ of the residual strain versus the number of cycles have been divided by the functions $\bar{f}_{ampl}$, $\bar{f}_e$, f_p and f_Y of the HCA model, in order to study the pure N-dependence of the accumulation rate. For both materials the data from the different tests fall together into a band, the scatter being slightly larger for the UGM.

For the pluviated sand samples, the curves run proportional to the number of cycles in the range $N \leq 10^4$ and over-proportional for larger N-values. The curves for the pre-compacted UGM samples are over-logarithmic from the beginning of a test. In the literature, some researchers (e.g. Lentz & Baladi [13], Duku et al. [6]) found accumulation curves obeying $\varepsilon^{acc} \sim \ln(N)$ whereas other studies (e.g. Marr & Christian [15]) suggested an increase of the residual strain faster than proportional to the logarithm of N. In [37] it has been shown that the shape of the curves $\varepsilon^{acc}(N)$ depends on the grain size distribution curve. While uniform sands show curves almost proportional to the number of cycles, the curvature increases with increasing coefficient of uniformity $C_u = d_{60}/d_{10}$.

The function f_N in Eq. (19) originally developed for sand describes well also the curves $\varepsilon^{acc}(N)$ for the UGM. The fitting of Eq. (19) to the data in Fig. 9 resulted in constants $C_{N1} = 3.6 \cdot 10^{-4}$, $C_{N2} = 0.43$ and $C_{N3} = 5.0 \cdot 10^{-5}$ for sand and $C_{N1} = 5.2 \cdot 10^{-4}$, $C_{N2} = 0.03$ and $C_{N3} = 1.3 \cdot 10^{-5}$ for UGM. For calculations with larger numbers of load cycles, the applicability of the function f_N should be checked for $N > 10^5$. For that purpose long-time tests with larger numbers of cycles are necessary. For sand, the over-logarithmic function f_N was confirmed in cyclic tests with $N = 2 \cdot 10^6$ cycles [33] and even larger numbers of cycles will be tested in future.

All constants of the HCA model have been summarized in Table 1.

6 Recalculation of the laboratory tests

The HCA model and the material constants given in Table 1 were used for recalculations of the laboratory tests. The initial densities, the average stresses and the measured strain amplitudes were used as input. The implementation of the HCA model in a Fortran code (user's subroutine UMAT for finite element calculations with the program ABAQUS) in conjunction with a Fortran routine for the calculation of element tests (so-called "Incremental driver", programmed by A. Niemunis) were used. Figure 10 presents a comparison of the calculated curves $\varepsilon^{acc}(N)$ with the experimental data for the sand and for the UGM. For both materials, most of the curves $\varepsilon^{acc}(N)$ measured for different amplitudes, densities, average mean pressures and average stress ratios are predicted well by the HCA model. Therefore, with the modifications and material constants proposed in this paper the HCA model is suitable also for the prediction of permanent deformations in UGM layers, at least for the stress and strain levels tested in the present study.

7 Summary and conclusions

The applicability of a high-cycle accumulation (HCA) model originally developed for sand for the prediction of permanent deformations in an unbound granular material

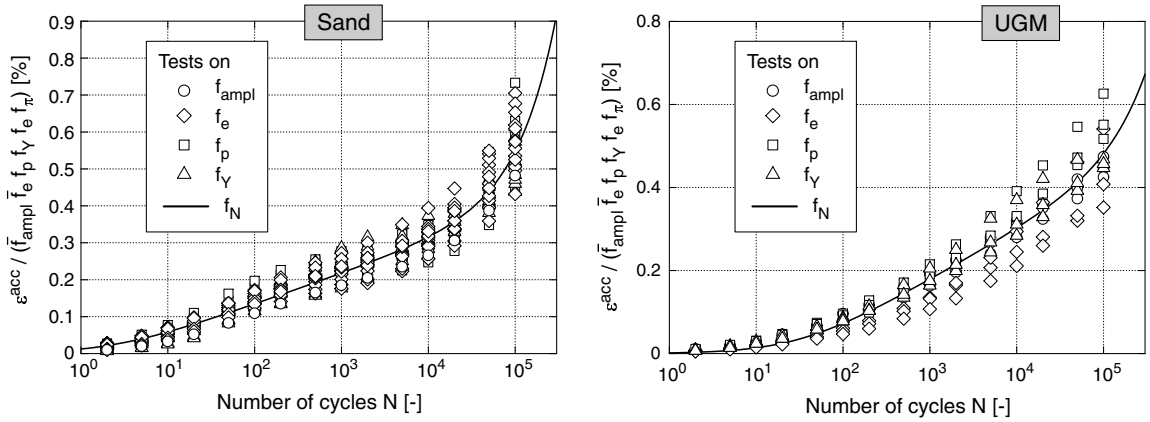

Fig. 9: *Accumulation curves $\varepsilon^{\mathrm{acc}}(N)$ divided by the functions $\bar{f}_{\mathrm{ampl}}$, $\bar{f}_e$, f_p and f_Y: N-dependence of the accumulation rate*

(UGM) used for base and subbase layers of pavements has been inspected. For that purpose cyclic triaxial tests on pre-compacted specimens of a typical UGM were performed. The results have been compared to those of air-pluviated sand specimens.

The functions f_{ampl}, f_e, f_p, f_Y and $\dot{f}_N$, used in the HCA model for the intensity of accumulation $\dot{\varepsilon}^{\mathrm{acc}}$, are suitable also for UGM, although the material constants differ from those obtained for sand. An increase of the intensity of accumulation with increasing strain amplitude, with decreasing initial density and with increasing average stress ratio $\eta^{\mathrm{av}} = q^{\mathrm{av}}/p^{\mathrm{av}}$ was observed for both materials. A significant difference was found regarding the exponent of the amplitude-dependence. It is 2.0 for sand but only 1.1 for UGM. Therefore, the proportionality between the accumulation rate and the square of the strain amplitude $(\varepsilon^{\mathrm{ampl}})^2$ observed for various sands does not apply to the UGM. The pressure-dependence of the accumulation rate is also different for UGM and for sand. If cycles with a constant strain amplitude are applied, the permanent strain accumulation decreases with increasing average mean pressure p^{av} for sand, while it increases for UGM. Therefore, for UGM the function f_p must be used with a negative value of the material constant C_p.

The isotropic flow rule used for the direction of accumulation for sand has been found insufficient for the UGM. A more generalized, anisotropic flow rule is necessary in order to describe the experimental observation that the accumulation is pure volumetric at an average stress ratio much larger than zero ($\eta^{\mathrm{av}} \approx 0.5$). Similar to sand, the pure deviatoric accumulation is expected at the critical state line. Equations for a generalized flow rule have been introduced in the paper.

Recalculations of the laboratory tests with the determined material constants confirmed a good prediction of the experimental data by the modified HCA model. Therefore, the modified HCA model may be a useful tool for studying more complicated boundary value problems in the field of pavement engineering, at least for the strain and stress levels studied in the present study.

References

[1] *DIN 18126: Bestimmung der Dichte nichtbindiger Böden bei lockerster und dichtester Lagerung*, 1996.

[2] *DIN EN 13286-7: Triaxial tests with cyclic loading for unbound granular material*, 2004.

[3] J.L. Chaboche. Modelling of ratchetting: evaluation of various approaches. *European Journal of Mechanics*, 13(4):501–518, 1994.

[4] C.S. Chang and R.V. Whitman. Drained permanent deformation of sand due to cyclic loading. *Journal of Geotechnical Engineering, ASCE*, 114(10):1164–1180, 1988.

[5] INVIAS Instituto Nacional de Vías. Especificaciones generales de construcción de carreteras. Bogotá D.C., Colombia, 2002.

[6] P.M. Duku, J.P. Stewart, D.H. Whang, and E. Yee. Volumetric strains of clean sands subject to cyclic loads. *Journal of Geotechnical and Geoenvironmental Engineering, ASCE*, 134(8):1073–1085, 2008.

[7] G. Gidel, D. Breysee, P. Hornych, J.-J. Chauvin, and A. Denis. A new approach for investigating the permanent deformation behaviour of unbound granular material using the repeated load triaxial apparatus. *Bulletin des Laboratoires des Ponts et Chaussées*, 233(4):5–21, 2001.

[8] S. Goto, F. Tatsuoka, S. Shibuya, Y.-S. Kim, and T. Sato. A simple gauge for local small strain measurements in the laboratory. *Soils and Foundations*, 31(1):169–180, 1991.

[9] S.J. Hain. An application of cyclic triaxial testing to field model test. In *International Symposium on Soils under cyclic and transient loading*, pages 23–31. Balkema, Rotterdam, Januar 1980. Swansea.

[10] M. Huurman. *Permanent deformation in concrete block pavements*. PhD thesis, Delft University of Technology, 1997.

[11] W.S. Kaggwa, J.R. Booker, and J.P. Carter. Residual strains in calcareous sand due to irregular cyclic loading. *Journal of Geotechnical Engineering, ASCE*, 117(2):201–218, 1991.

[12] F. Lekarp, U. Isacsson, and A. Dawson. State of the art. I: Resilient response of unbound aggregates. *Journal of Transportation Engineering*, 126(1):66–75, 2000.

[13] R.W. Lentz and G.Y. Baladi. Simplified procedure to characterize permanent strain in sand subjected to cyclic loading. In *International Symposium on soils under cyclic and transient loading*, pages 89–95. Balkema, Rotterdam, Januar 1980.

[14] M.P. Luong. Mechanical aspects and thermal effects of cohesionless soils under cyclic and transient loading. In *Proc. IUTAM Conf. on Deformation and Failure of Granular materials, Delft*, pages 239–246, 1982.

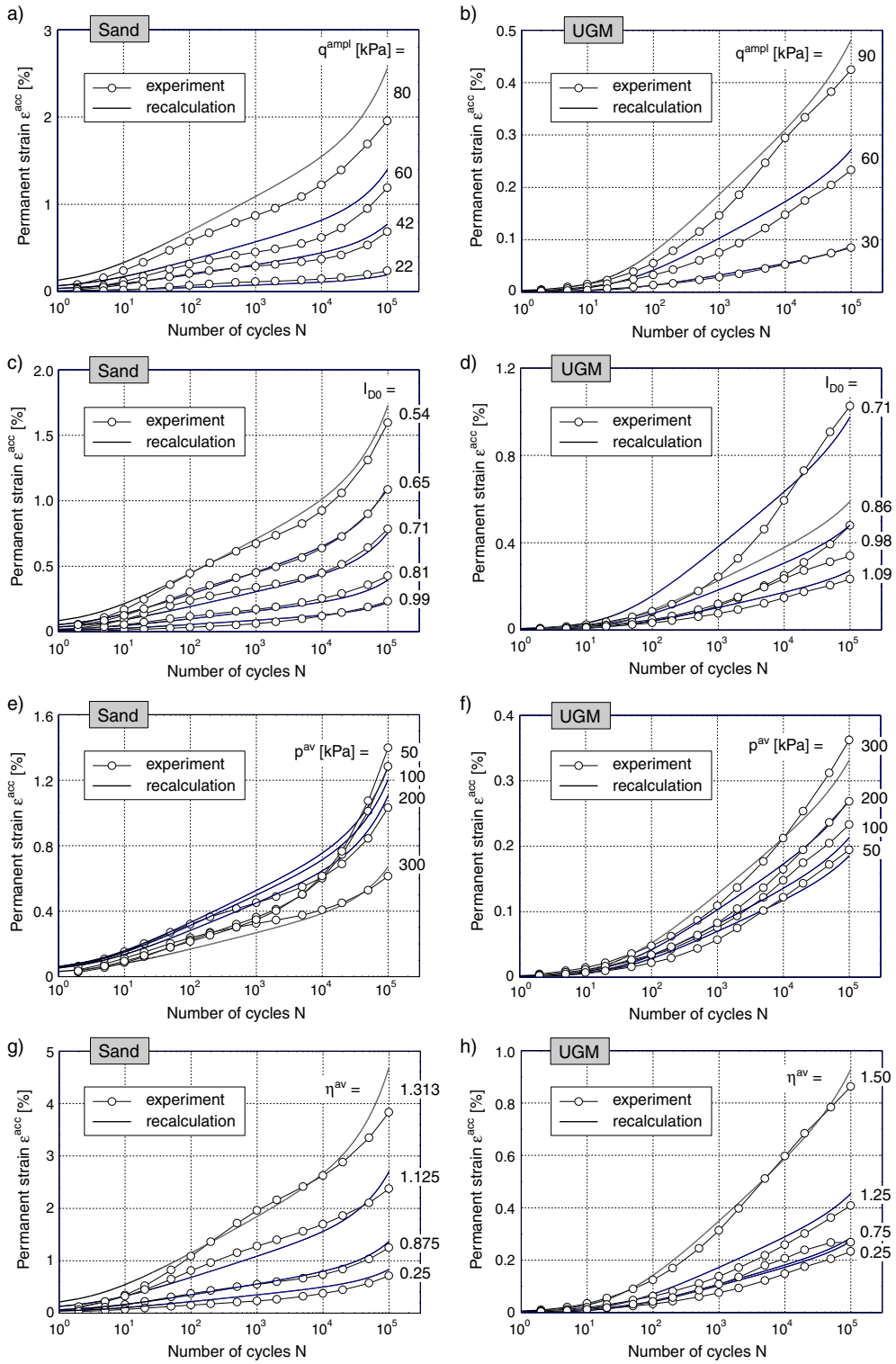

Fig. 10: *Recalculation of the laboratory tests using the HCA model and the material constants summarized in Table 1*

[15] W.A. Marr and J.T. Christian. Permanent displacements due to cyclic wave loading. *Journal of the Geotechnical Engineering Division, ASCE*, 107(GT8):1129–1149, 1981.

[16] H. Matsuoka and T. Nakai. A new failure criterion for soils in three-dimensional stresses. In *Deformation and Failure of Granular Materials*, pages 253–263, 1982. Proc. IUTAM Symp. in Delft.

[17] M. Miner. Cumulative damage in fatigue. *Transactions of the American Society of Mechanical Engineering*, 67:A159–A164, 1945.

[18] Z. Mróz, V.A. Norris, and O.C. Zienkiewicz. An anisotropic hardening model for soils and its application to cyclic loading. *Int. J. Numer. Anal. Meth. Geomech.*, 2:203–221, 1978.

[19] A. Niemunis and I. Herle. Hypoplastic model for cohesionless soils with elastic strain range. *Mechanics of Cohesive-Frictional Materials*, 2:279–299, 1997.

[20] A. Niemunis, T. Wichtmann, and T. Triantafyllidis. A high-cycle accumulation model for sand. *Computers and Geotechnics*, 32(4):245–263, 2005.

[21] R. Pyke, H.B. Seed, and C.K. Chan. Settlement of sands under multidirectional shaking. *Journal of the Geotechnical Engineering Division, ASCE*, 101(GT4):379–398, 1975.

[22] H. A. Rondón and F. A. Reyes. *Comportamiento de materiales granulares en pavimentos flexibles: estado del conocimiento*. Universidad Católica de Colombia y Pontificia Universidad Javeriana, Bogotá D.C., 2008.

[23] H. A. Rondón, T. Wichtmann, Th. Triantafyllidis, and A. Lizcano. Comparison of cyclic triaxial behavior of unbound granular material under constant and variable confining pressure. *Journal of Transportation Engineering*, 135(7):467–478, 2009.

[24] A. Sawicki and W. Świdziński. Compaction curve as one of basic characteristics of granular soils. In E. Flavigny and D. Cordary, editors, *4th Colloque Franco-Polonais de Mechanique des Sols Appliquee*, volume 1, pages 103–115, 1987. Grenoble.

[25] A. Sawicki and W. Świdziński. Mechanics of a sandy subsoil subjected to cyclic loadings. *Int. J. Numer. Anal. Meth. Geomech.*, 13:511–529, 1989.

[26] M.J. Shenton. Deformation of Railway Ballast under repeated loading conditions. Railroad track mechanics and technology. *Pergamon Press*, pages 405–425, 1978.

[27] M.L. Silver and H.B. Seed. Deformation characteristics of sands under cyclic loading. *Journal of the Soil Mechanics and Foundations Division, ASCE*, 97(SM8):1081–1098, 1971.

[28] M.L. Silver and H.B. Seed. Volume changes in sands during cyclic loading. *Journal of the Soil Mechanics and Foundations Division, ASCE*, 97(SM9):1171–1182, 1971.

[29] T. Triantafyllidis, T. Wichtmann, and A. Niemunis. On the determination of cyclic strain history. In Triantafyllidis, editor, *Cyclic Behaviour of Soils and Liquefaction Phenomena, Proc. of CBS04, Bochum*, pages 321–332. Balkema, 31 March - 02 April 2004.

[30] J. Uzan. Permanent Deformation in Flexible Pavements. *Journal of Transportation Engineering*, 130:6 – 13, 2004.

[31] P.-A. von Wolffersdorff. A hypoplastic relation for granular materials with a predefined limit state surface. *Mechanics of Cohesive-Frictional Materials*, 1:251–271, 1996.

[32] S. Werkmeister, A. Dawson, and F. Wellner. Pavement Design Model of Unbound Granular Materials. *Journal of Transportation Engineering*, 130:665 – 674, 2004.

[33] T. Wichtmann. Explicit accumulation model for non-cohesive soils under cyclic loading. PhD thesis, Publications of the Institute of Soil Mechanics and Foundation Engineering, Ruhr-University Bochum, Issue No. 38, available from www.rz.uni-karlsruhe.de/∼gn97/, 2005.

[34] T. Wichtmann, A. Niemunis, and T. Triantafyllidis. Strain accumulation in sand due to cyclic loading: drained triaxial tests. *Soil Dynamics and Earthquake Engineering*, 25(12):967–979, 2005.

[35] T. Wichtmann, A. Niemunis, and T. Triantafyllidis. On the influence of the polarization and the shape of the strain loop on strain accumulation in sand under high-cyclic loading. *Soil Dynamics and Earthquake Engineering*, 27(1):14–28, 2007.

[36] T. Wichtmann, A. Niemunis, and T. Triantafyllidis. Strain accumulation in sand due to cyclic loading: drained cyclic tests with triaxial extension. *Soil Dynamics and Earthquake Engineering*, 27(1):42–48, 2007.

[37] T. Wichtmann, A. Niemunis, and T. Triantafyllidis. Validation and calibration of a high-cycle accumulation model based on cyclic triaxial tests on eight sands. *Soils and Foundations*, 49(5):711–728, 2009.

[38] T. Wichtmann, A. Niemunis, and T. Triantafyllidis. On the determination of a set of material constants for a high-cycle accumulation model for non-cohesive soils. *Int. J. Numer. Anal. Meth. Geomech.*, 34(4):409–440, 2010.

[39] Y. Yamada and K. Ishihara. Yielding of loose sand in three-dimensional stress conditions. *Soils and Foundations*, 22(3):15–31, 1982.

[40] T.L. Youd. Compaction of sands by repeated shear straining. *Journal of the Soil Mechanics and Foundations Division, ASCE*, 98(SM7):709–725, 1972.